

Design of a silicon nitride photonic crystal nanocavity with a Quality factor of one million for coupling to a diamond nanocrystal

Murray W. McCutcheon and Marko Lončar

School of Engineering and Applied Science, Harvard University, Cambridge, MA, 02138
murray@seas.harvard.edu

Abstract: A photonic crystal nanocavity with a Quality (Q) factor of 1.4×10^6 , a mode volume of $0.78(\lambda/n)^3$, and an operating wavelength of 637 nm is designed in a silicon nitride (SiN_x) ridge waveguide with refractive index of 2.0. The effect on the cavity Q factor and mode volume of single diamond nanocrystals of various sizes and locations embedded in the center and on top of the nanocavity is simulated, demonstrating that $Q > 1 \times 10^6$ is achievable for realistic parameters. An analysis of the figures of merit for cavity quantum electrodynamics reveals that strong coupling between an embedded diamond nitrogen-vacancy center and the cavity mode is achievable for a range of cavity dimensions.

© 2008 Optical Society of America

OCIS codes: (230.5298) Photonic crystals; (230.5750) Optical devices, resonators; (270.5580) Quantum electrodynamics

References and links

1. R. Miller, T. E. Northrup, K. M. Birnbaum, A. Boca, A. D. Boozer, and H. J. Kimble, "Trapped atoms in cavity QED: coupling quantized light and matter," *J. Phys. B* **38**, S551–S565 (2005).
2. H. Walther, B. T. H. Varcoe, B.-G. Englert, and T. Becker, "Cavity quantum electrodynamics," *Rep. Prog. Phys.* **69**, 1325–1382 (2006).
3. C. Weisbuch, M. Nishioka, A. Ishikawa, and Y. Arakawa, "Observation of the coupled exciton-photon mode splitting in a semiconductor quantum microcavity," *Phys. Rev. Lett.* **69**, 3314–3317 (1992).
4. T. Yoshie, A. Scherer, J. Hendrickson, G. Khitrova, H. M. Gibbs, G. Rupper, C. Ell, O. B. Shchekin, and D. G. Deppe, "Vacuum Rabi splitting with a single quantum dot in a photonic crystal nanocavity," *Nature* **432**, 200–203 (2004).
5. J. P. Reithmaier, G. Sek, A. Löffler, C. Hofmann, S. Kuhn, S. Reitzenstein, L. V. Keldysh, V. D. Kulakovskii, T. L. Reinecke, and A. Forchel, "Strong coupling in a single quantum dot-semiconductor microcavity system," *Nature* **432**, 197–200 (2004).
6. K. Hennessy, A. Badolato, M. Winger, D. Gerace, M. Atature, S. Gulde, S. Falt, E. L. Hu, and A. Imamoglu, "Quantum nature of a strongly coupled single quantum dot-cavity system," *Nature* **445**, 896–899 (2007).
7. K. Srinivasan and O. Painter, "Linear and nonlinear optical spectroscopy of a strongly coupled microdisk-quantum dot system," *Nature* **450**, 862–865 (2007).
8. D. Englund, A. Faraon, I. Fushman, N. Stoltz, P. Petroff, and J. Vučković, "Controlling cavity reflectivity with a single quantum dot," *Nature* **450**, 857–861 (2007).
9. L. Childress, M. V. G. Dutt, J. M. Taylor, A. S. Zibrov, F. Jelezko, J. Wrachtrup, P. R. Hemmer, and M. D. Lukin, "Coherent dynamics of coupled electron and nuclear spins in diamond," *Science* **314**, 281–285 (2006).
10. C. Kurtsiefer, S. Mayer, P. Zarda, and H. Weinfurter, "Stable solid-state source of single photons," *Phys. Rev. Lett.* **85**, 290–293 (2000).
11. T. Gaebel, M. Domhan, I. Popa, C. Wittmann, P. Neumann, F. Jelezko, J. R. Rabeau, N. Stavrias, A. D. Greentree, S. Praver, J. Meijer, J. Twamley, P. R. Hemmer, and J. Wrachtrup, "Room-temperature coherent coupling of single spins in diamond," *Nature Physics* **2**, 408–413 (2006).

12. M. V. G. Dutt, L. Childress, L. Jiang, E. Togan, J. Maze, F. Jelezko, A. S. Zibrov, P. R. Hemmer, and M. D. Lukin, "Quantum register based on individual electronic and nuclear spin qubits in diamond," *Science* **316**, 1312–1316 (2007).
13. C. Santori, P. Tamarat, P. Neumann, J. Wrachtrup, D. Fattal, R. G. Beausoleil, J. Rabeau, P. Olivero, A. D. Greentree, S. Praver, F. Jelezko, and P. Hemmer, "Coherent population trapping of single spins in diamond under optical excitation," *Phys. Rev. Lett.* **97**, 247401 (2006).
14. R. Hanson, F. M. Mendoza, R. J. Epstein, and D. D. Awschalom, "Polarization and readout of coupled single spins in diamond," *Phys. Rev. Lett.* **97**, 087601 (2006).
15. J. Meijer, B. Burchard, M. Domhan, C. Wittmann, T. Gaebel, I. Popa, F. Jelezko, and J. Wrachtrup, "Generation of single color centers by focused nitrogen implantation," *Appl. Phys. Lett.* **87**, 261909 (2005).
16. F. Jelezko, T. Gaebel, I. Popa, M. Domhan, A. Gruber, and J. Wrachtrup, "Observation of coherent oscillations in a single electron spin," *Phys. Rev. Lett.* **92**, 076401 (2004).
17. A. D. Greentree, J. Salzman, S. Praver, and L. C. L. Hollenberg, "Quantum gate for Q switching in monolithic photonic-band-gap cavities containing two-level atoms," *Phys. Rev. A* **73**, 013818 (2006).
18. J. I. Cirac, P. Zoller, H. J. Kimble, and H. Mabuchi, "Quantum state transfer and entanglement distribution among distant nodes in a quantum network," *Phys. Rev. Lett.* **78**, 3221–3224 (1997).
19. S. J. van Enk, J. I. Cirac, and P. Zoller, "Ideal quantum communication over noisy channels: A quantum optical implementation," *Phys. Rev. Lett.* **78**, 4293–4296 (1997).
20. Y. Shen, T. M. Sweeney, and H. Wang, "Zero-phonon linewidth of single nitrogen vacancy centers in diamond nanocrystals," *Phys. Rev. B* **77**, 033201 (2008).
21. Y.-S. Park, A. K. Cook, and H. Wang, "Cavity QED with diamond nanocrystals and silica microspheres," *Nano Lett.* **6**, 2075–2079 (2006).
22. S. Tomljenovic-Hanic, M. J. Steel, and C. M. de Sterke, "Diamond based photonic crystal microcavities," *Opt. Express* **14**, 3556–3562 (2006).
23. C. Kreuzer, J. Riedrich-Moller, E. Neu, and C. Becher, "Design of photonic crystal microcavities in diamond films," *Opt. Express* **16**, 1632–1644 (2008).
24. I. Bayn and J. Salzman, "Ultra high- Q photonic crystal nanocavity design: The effect of a low-index slab material," *Opt. Express* **16**, 4972 (2008).
25. C. F. Wang, R. Hanson, D. D. Awschalom, E. L. Hu, T. Feygelson, J. Yang, and J. E. Butler, "Fabrication and characterization of two-dimensional photonic crystal microcavities in nanocrystalline diamond," *Appl. Phys. Lett.* **91**, 201112 (2007).
26. K. Rivoire, A. Faraon, and J. Vučković, "Gallium phosphide photonic crystal nanocavities in the visible," *Appl. Phys. Lett.* **93**, 063103 (2008).
27. P. E. Barclay, K. Srinivasan, O. Painter, B. Lev, and H. Mabuchi, "Integration of fiber-coupled high- Q SiN_x microdisks with atom chips," *Appl. Phys. Lett.* **13**, 801 (2005).
28. M. Eichenfeld, C. P. Michael, R. Perahia, and O. Painter, "Actuation of micro-optomechanical systems via cavity-enhanced optical dipole forces," *Nature Photonics* **1**, 416–422 (2007).
29. B. S. Song, S. Noda, T. Asano, and Y. Akahane, "Ultra-high- Q photonic double-heterostructure nanocavity," *Nature Materials* **4**, 207–210 (2005).
30. E. Kuramochi, M. Notomi, S. Mitsugi, A. Shinya, T. Tanabe, and T. Watanabe, "Ultrahigh- Q photonic crystal nanocavities realized by the local width modulation of a line defect," *Appl. Phys. Lett.* **88**, 041112 (2006).
31. M. Barth, N. Nüsse, J. Stingl, B. Lochel, and O. Benson, "Emission properties of high- Q silicon nitride photonic crystal heterostructure cavities," *Appl. Phys. Lett.* **93**, 021112 (2008).
32. P. Lalanne and J. P. Hugonin, "Bloch-wave engineering for high- Q , small- V microcavities," *IEEE J. Quantum Electron.* **39**, 1430–1438 (2003).
33. P. Lalanne and S. M. J. P. Hugonin, "Two physical mechanisms for boosting the quality factor to cavity volume ratio of photonic crystal microcavities," *Opt. Express* **12**, 458–467 (2004).
34. C. Sauvan, G. Lecamp, P. Lalanne, and J. Hugonin, "Modal-reflectivity enhancement by geometry tuning in photonic crystal microcavities," *Opt. Express* **13**, 245–255 (2005).
35. M. Barth, J. Kouba, J. Stingl, B. Lochel, and O. Benson, "Modification of visible spontaneous emission with silicon nitride photonic crystal nanocavities," *Opt. Express* **15**, 17231–17240 (2007).
36. We use Lumerical FDTD Solutions for all our simulations .
37. O. Painter, J. Vučković, and A. Scherer, "Defect modes of a two-dimensional photonic crystal in an optically thin dielectric slab," *J. Opt. Soc. Am. B* **16**, 275–285 (1999).
38. M. Borselli, T. J. Johnson, and O. Painter, "Beyond the Rayleigh scattering limit in high- Q silicon microdisks: theory and experiment," *Opt. Express* **13**, 1515–1530 (2005).
39. M. Notomi, E. Kuramochi, and H. Taniyama, "Ultrahigh- Q nanocavity with 1D photonic gap," *Opt. Express* **16**, 11095–11102 (2008).
40. Y. Zhang and M. Lončar, "Ultra-high quality factor optical resonators based on semiconductor nanowires," *Opt. Express* **16**, 17400–17409 (2008).
41. J. Vučković, M. Lončar, H. Mabuchi, and A. Scherer, "Design of photonic crystal microcavities for cavity QED," *Phys. Rev. E* **65**, 016608 (2001).
42. J. Vučković, M. Lončar, H. Mabuchi, and A. Scherer, "Optimization of the Q factor in photonic crystal micro-

- cavities," *IEEE J. Quantum Electron.* **38**, 850–856 (2002).
43. A. R. M. Zain, M. Gnan, H. M. H. Chong, M. Sorel, and R. M. D. L. Rue, "Tapered photonic crystal microcavities embedded in photonic wire waveguides with large resonance Quality-factor and high transmission," *IEEE Photon. Technol. Lett.* **20**, 6–8 (2008).
 44. K. Hennessy, A. Badolato, P. M. Petroff, and E. L. Hu, "Positioning photonic crystal cavities to single InAs quantum dots," *Photonics and Nanostructures* **2**, 65–72 (2004).
 45. A. Badolato, K. Hennessy, M. Atature, J. Dreiser, E. Hu, P. M. Petroff, and A. Imamoglu, "Deterministic coupling of single quantum dots to single nanocavity modes," *Science* **308**, 1158–1161 (2005).
 46. A. F. Koenderink, M. Kafesaki, C. M. Soukoulis, and V. Sandoghdar, "Spontaneous emission in the near field of two-dimensional photonic crystals," *Opt. Lett.* **30**, 3210–3212 (2005).
 47. A. Bevaratos, S. Kuhn, R. Brouri, T. Gacoin, J.-P. Poizat, and P. Grangier, "Room temperature stable single-photon source," *Eur. Phys. J. D* **18**, 191–196 (2002).
 48. J.-M. Gérard, "Solid-state cavity-quantum electrodynamics with self-assembled quantum dots" in *Single quantum dots: fundamentals, applications, and new concepts*, P. Michler ed. (Springer, 2003), pp. 269–314.
 49. P. E. Barclay, "Fiber-coupled nanophotonic devices for nonlinear optics and cavity QED," PhD. Thesis, California Institute of Technology (2007).
 50. P. Tamarat, T. Gaebel, J. R. Rabeau, M. Khan, A. D. Greentree, H. Wilson, L. C. L. Hollenberg, S. Prawer, P. Hemmer, F. Jelezko, and J. Wrachtrup, "Stark shift control of single optical centers in diamond," *Phys. Rev. Lett.* **97**, 083002 (2006).
 51. M. G. Banaee, A. G. Pattantyus-Abraham, M. W. McCutcheon, G. W. Rieger, and J. F. Young, "Efficient coupling of photonic crystal microcavity modes to a ridge waveguide," *Appl. Phys. Lett.* **90**, 193106 (2007).
 52. T. Tanabe, M. Notomi, E. Kuramochi, A. Shinya, and H. Taniyama, "Trapping and delaying photons for one nanosecond in an ultrasmall high- Q photonic-crystal nanocavity," *Nature Photonics* **1**, 49–52 (2007).
 53. M. W. McCutcheon, A. G. Pattantyus-Abraham, G. W. Rieger, and J. F. Young, "Emission spectrum of electromagnetic energy stored in a dynamically perturbed optical microcavity," *Opt. Express* **15**, 11472–11480 (2007).

1. Introduction

Recently there has been much interest in solid-state approaches to the study of quantum information, light-matter interactions and cavity quantum electrodynamics (QED) [1, 2]. There are many potential advantages to implementing quantum protocols on a semiconductor chip. The dipole coupling of matter to the field can be fixed because of the monolithic nature of the design. Moreover, an integrated design can be naturally coupled to other on-chip devices, both photonic and electronic, and is inherently scalable. Strong coupling experiments in solid-state cavity QED have evolved from the 1D geometry of quantum wells in a Fabry-Perot microcavity [3] to full three-dimensionally confining micropillar and photonic crystal microcavities coupled to epitaxial quantum dots [4, 5]. More recently, there have been a number of significant advances [6, 7, 8] in both photonic crystal cavities and microdisks.

Single nitrogen-vacancy (NV) defect centers in diamond have recently emerged as promising candidates for quantum optics and quantum information [9]. They act as stable sources of single photons [10], and at room temperature, they have electron spin coherence times of 350 μ s [11] and nuclear spin coherence times of 0.5 ms. These spin states can be manipulated to form a quantum register [12], and coupled with reasonable strength to optical transitions such as the zero-phonon line (ZPL), allowing the read-out of the state [13, 14]. NV centers occur naturally in bulk diamond, but their spin states can dephase in the presence of proximate nitrogen spins. Recently, techniques have been developed to artificially implant NV centers in high-purity single crystal diamond, which limits the density of substitutional nitrogen atoms and the associated sources of decoherence [11, 15]. Although much of this research relates to bulk diamond, NV centers embedded in 20 nm sized diamond nanocrystals (NCs) have also been shown to have spin coherence times on the order of microseconds [16]. Embedding these diamond NCs in an optical microcavity could allow realization of the coherent light-matter interactions crucial for certain quantum protocols. With an appropriately designed cavity, for example, this coherence could be controlled and entangled with photon states for transfer of the quantum information [17, 18, 19], provided the candidate NV center is not limited by spectral diffusion or dark states [20]. In fact, diamond NCs of about 75 nm in size have been strongly

coupled to the whispering gallery modes of silica microspheres [21].

Our goal is to design a wavelength-scale microcavity for coupling to diamond NCs on a planar platform, which would facilitate integration with other optical devices. A major challenge in realizing strongly-coupled diamond NV centers in this system is the fact that the ZPL optical transition is in the visible (637 nm for the negatively charged NV^- center). A monolithic nanocavity must therefore be designed in a visibly transparent material. One option is diamond, which has a reasonably high refractive index $n = 2.43$, and optical resonators have been designed for thin slabs of diamond [22, 23] with $Q > 10^6$ [24]. Experimentally this is very challenging, as the growth of single crystal diamond slabs has yet to be realized, and the polycrystalline films which are readily available suffer from large scattering losses which has limited the measured Q factors to less than 1000 [25]. In bulk single crystal diamond, moreover, it is difficult to realize these structures due to the considerable challenge of creating three-dimensionally confining defect cavities.

For material systems operating in the visible, an alternative to diamond is a wide bandgap material, such as silicon nitride, hafnium oxide, gallium nitride, or gallium phosphide [26]. Silicon nitride and hafnium oxide are particularly promising candidates because of their compatibility with advanced silicon nanofabrication processes. Indeed, SiN_x microdisks have been fabricated with $Q = 3.6 \times 10^6$ and mode volumes $V = 15(\lambda/n)^3$ [27, 28]. The moderately low refractive index of ~ 2.0 of SiN_x has often been considered an impediment to ultra-high- Q photonic crystal nanocavity designs, which thusfar have only been demonstrated in high index semiconductors such as silicon [29, 30]. To wit, the highest reported photonic crystal cavity design in SiN_x has yielded a Q factor of 12,900 with a mode volume of $1.62(\lambda/n)^3$ [31].

In this paper, we demonstrate a silicon nitride photonic crystal nanocavity design with a Q factor of 1.4×10^6 and a mode volume of $\sim 0.78(\lambda/n)^3$. Considering the relative ease of fabrication and the natural integration of our design as part of an on-chip ridge waveguide, this remarkably high Q/V ratio renders this device as a highly promising platform on which to pursue visible solid-state cavity QED. Although we focus on silicon nitride, these results are applicable for any low-loss material with $n \sim 2.0$.

We first discuss our systematic approach to engineer the nanocavity, which is based on a series of publications by Lalanne et al. [32, 33, 34]. We then consider the effect on the mode Q factor of a diamond NC embedded in the center of the cavity or positioned on top of the cavity surface. We demonstrate that a Q factor greater than 80% of the bare cavity Q is obtainable for a realistic NC size of 20 nm embedded in our highest Q cavity. For the case of the NC on top of the cavity, we explore the effect of spatial location of the NC with respect to the mode center, and evaluate the effect on the mode Q . We then evaluate the cavity QED figures of merit and show that when the NC is embedded in the center of the cavity, the system is capable of realizing the strong coupling limit.

2. Cavity design

Because of the relatively low index of refraction ($n = 2.0$) of SiN_x , the two-dimensional photonic bandgap of SiN_x planar photonic crystal slabs is small, particularly when measured against a high index semiconductor like silicon. This makes the design of nanocavities in 2D photonic lattices challenging [35, 31]. To circumvent this difficulty, we consider a nanocavity for which the photonic lattice provides only one dimensional (1D) confinement, and total internal reflection provides the confinement mechanism in the other two dimensions (2D). A sketch of our 1D nanocavity is shown in Fig. 1, which also shows a 60 nm diamond nanocrystal positioned on top of the cavity.

The design process consists of engineering three elements: (a) the photonic crystal mirror, (b) the taper, and (c) the cavity length. We consider a free-standing SiN_x ridge waveguide of thickness 200 nm and width 300 nm which supports a single TE mode. These parameters

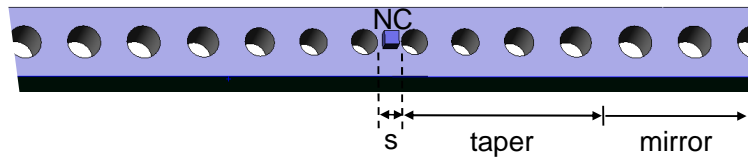


Fig. 1. Sketch of the 1D photonic crystal waveguide nanocavity, showing a 60 nm diamond nanocrystal located on top of a cavity of length s . The taper and photonic crystal mirror sections are symmetric about the cavity center.

are chosen as representative of our experimental wafer, and have not been optimized in any fashion. The photonic crystal mirror parameters, namely the hole spacing $a = 250$ nm and radius $r = 0.28a$, are chosen to center the resulting stop-band around the wavelength of interest (~ 637 nm). We can characterize the reflectivity of the mirror using the 3D finite-difference time-domain (FDTD) method by launching a waveguide mode pulse and monitoring the reflection spectrum.

As shown by Sauvan et al. [34], the scattering losses arise in part from the mode mismatch between the waveguide and Bloch mirror modes. The mismatch can be quantified by comparing the effective index of the Bloch mode, $n_{\text{Bl}} = \lambda/2a$, to the effective index of the waveguide mode, n_{wg} (determined using our 3D-FDTD mode solver [36]). By tapering the hole-spacing in the mirror, n_{Bl} can be smoothly increased to the value of n_{wg} , allowing for an adiabatic transition between the modes in the two regions. The r/a ratio is maintained close to that of the uniform mirror throughout the taper.

We gauge the efficacy of linear tapers up to 7 holes in length with a 17 hole mirror according to the magnitude of the loss, as plotted in Fig. 2(a). Each increase in the taper length has the effect of further reducing the mismatch between mirror and waveguide, resulting in a loss suppression of more than one order of magnitude between the 7-hole taper and untapered mirror.

The nanocavity is defined by the gap s between two taper/mirror sections, as shown in Fig. 1. In the 3D-FDTD simulation, the Q factor is determined from the exponential decay of the electric field ringdown in the cavity, and this agrees well with the value determined by monitoring the mode energy and the power absorbed by the simulation boundaries [37]. The Q factors (circles) are plotted as a function of the nanocavity length, s , for both the 4-hole and 7-hole tapers in Fig. 2(b). As expected from the data in Fig. 2(a), the 7-hole taper yields the maximum Q of 1.4×10^6 . This is two orders of magnitude greater than the best PhC cavity design in the literature to date for a material with refractive index as low as 2.0 [31]. In these simulations, we have not considered material absorption, which was shown by Barclay et al. [27, 38] to be a limiting factor in SiN_x only for Q factors greater than 3 million, or scattering due to fabrication imperfections. Further optimization may be possible by optimizing the waveguide width and thickness, as well as using different taper forms.

The mode volumes are plotted with the square symbols in Fig. 2(b). The cavity with the maximum Q has a mode volume $\sim 0.78(\lambda/n)^3$. Despite the relatively low refractive index of SiN_x , this is smaller than the effective mode volume of the recent ultra-high- Q photonic crystal cavities designed in high index semiconductors [29, 30, 39]. This can be attributed in part to the fact that our cavity operates at the mid-gap frequency, where the loss is minimum (see Fig. 2(a)), and demonstrates the highly attractive ultra-small size of our nanocavity.

The mechanism which yields the high Q factor in the 7-hole tapered nanocavities is more subtle than a simple reduction of mirror loss compared to the shorter tapers. Compared to a Fabry-Perot cavity, the difference here is that the cavity mode is derived from the propagating Bloch modes of the photonic crystal mirror, and the local structural perturbation which forms

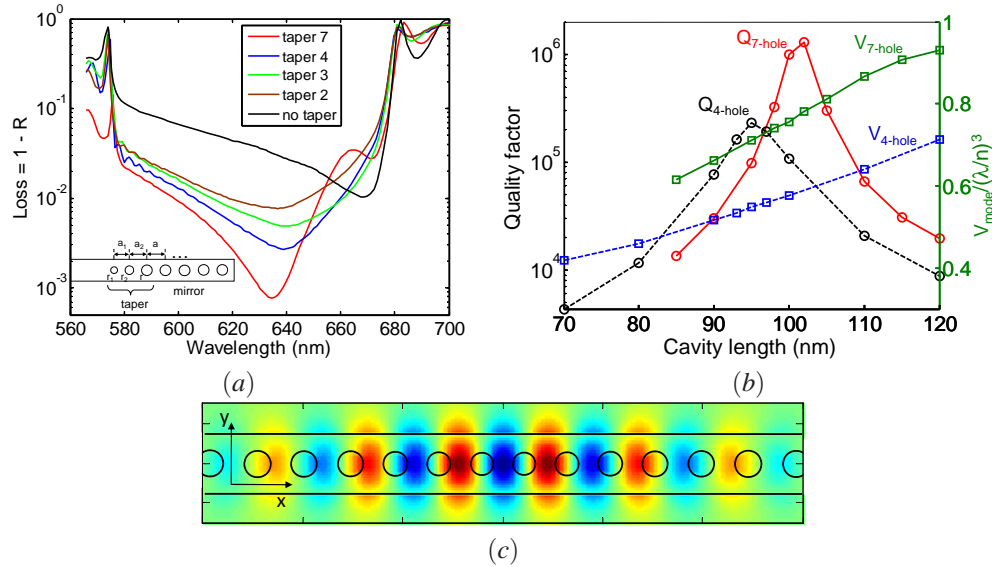


Fig. 2. (a) Loss parameter for 5 different designs of photonic crystal mirrors. The inset defines the hole pitch (a) and radii (r). For each taper design, r is linearly increased from 55 to 70 nm, and a from 214 to 250 nm. (b) Quality factor (circles) and effective mode volume (squares) as a function of cavity length for a free-standing PhC ridge waveguide in SiN_x with a 4-hole and 7-hole taper and a 17 period mirror. (c) Cavity mode electric field (E_y) for the 7-hole taper cavity with $Q = 1.4 \times 10^6$.

the cavity introduces a mode gap [39, 29, 43] capable of supporting very high Q modes. Recently, we used a similar approach to design cavities based on semiconductor nanowires with $Q \sim 10^6$ [40]. The tapered transition from the mirror to the nanocavity not only reduces mirror loss in the simple Fabry-Perot picture, but reduces radiative loss arising from delocalization of the mode profile in k -space [41, 42]. There may also be a role played by radiation modes in recycling the mirror losses and increasing the Q factor [33].

3. Incorporation of a diamond nanocrystal

Now that we have optimized our photonic crystal nanocavity design, we consider exploiting this nanocavity to enhance the zero-phonon line (ZPL) emission from a NV center in a diamond nanocrystal. Coupling the emission to the nanocavity mode will lead to a Purcell enhancement of the spontaneous emission rate, and as we show below, the potential to realize quantum dynamics in the strong coupling regime.

The ideal placement of the diamond NC is in the middle of the nanocavity, where the NV center can interact with the maximal electric field of the cavity mode. It is important to quantify the effect of the NC on the cavity Q factor. A 5 nm mesh grid is used in the central part of the simulation in order to accurately model the effects of the small volume of diamond. We consider 20 nm and 40 nm sized cubic diamond NCs in conjunction with the 4-hole taper design. Interestingly, the results reveal that the Q factor is not uniformly affected for all cavities. For cavities longer than 95 nm incorporating a 20 nm NC, the Q decreases by 10-12%, but for cavities shorter than this, the Q factor is actually *increased*. In the best 4-hole taper cavity ($s = 95$ nm), the bare Q factor of 230,000 increases to 240,000 with the 20 nm NC. These results perhaps reflect a trade-off between the beneficial impact of the increased refractive index in the cavity center, which would be expected to raise the Q factor, and the deleterious effect of

changing the impedance matching condition used to design the mirror tapers. As expected with the higher index cavity core, there is a reduction of about 10% in the mode volume for all cavity lengths. We conducted a similar investigation for a 40 nm cubic diamond NC located at the cavity center, and found that the Q vs. s curve shifts to shorter cavities compared to the 4-hole taper results in Fig. 2(b), yielding a peak $Q = 260,000$ at $s = 90$ nm, with a mode volume of $0.50 (\lambda/n)^3$. For the 7-hole taper design, the Q factors for cavities with an embedded 20 nm NC are about 20% smaller than in the unperturbed cavities, showing that scattering effects play a more substantial role in these higher Q cavities. The mode volumes, in turn, are decreased by 20%. The main conclusion that can be drawn from this analysis is that the cavity Q factors and mode volumes are not changed substantially ($\sim 10 - 20\%$) from the bare cavity values when a 20 nm NC is embedded in the cavity center.

Experimentally, an embedded NC might be realized by depositing a 100 nm layer of SiN_x on a sacrificial layer of SiO_2 , placing a single diamond NC in a known position, and then depositing another 100 nm layer of SiN_x to cap the structure and embed the NC in the middle. The NC position could be registered with respect to external alignment markers [44], or the position might be revealed after the SiN_x regrowth by a bump on the top surface [45]. The PhC nanocavity would then be patterned around the NC, followed by removal of the SiO_2 . We simulated the scenario of a small 20 nm bump of SiN_x on top of the 4-hole taper cavity with an embedded 20 nm NC, and found a reduction of only about 2% in the Q factor of the best cavity.

An alternate approach to embedding a diamond NC would be to position the NC on top of the cavity. In [46], Koenderink et al. consider the emission enhancement of a dipole right at the semiconductor/air interface of a uniform slab 2D photonic crystal, and show that the rate can be enhanced by 5 - 10 times near the band edges. Here we model a similar scenario, except the emitter is situated on the top surface of our SiN_x nanocavity. The high Q/V ratio of our nanocavity presents the possibility to yield much higher emission enhancements, as elaborated below, with a maximum Purcell factor of 7,000 for the NC on top of, and 10^5 for the NC embedded within, the optimal 7-hole taper cavity.

We consider diamond NC cubes with 3 different edge lengths: 20 nm, 40 nm, and 60 nm, and consider the effect of such a NC placed exactly above the central anti-node of the nanocavity mode. We explore the effect on the mode Q factor of this small dielectric perturbation ($n = 2.43$), and analyze the sensitivity of the Q to the precise positioning of the NC. The 4-hole taper cavity design for these simulations had a maximum Q of 115,000 ($s = 100$ nm), which was not the optimal design. The simulations are repeated for a range of NC positions to model the effect of imperfect NC placement, and the results are summarized in Fig. 3. The NC position is varied over a displacement of 40 nm in the x -direction and 60 nm in the y -direction with respect to the center of the cavity, as shown by the white box in Fig. 3(a).

The results show that while the relatively large 60 nm diamond NCs have a significant impact on the mode Q , the situation is very promising for 40 nm and 20 nm sized NCs. The on-center Q factor is 47,000 for a 40 nm NC, and as the position is moved away in either the x or y directions from the mode center, the Q factor increases to a maximum of almost 74,000 at $(x, y) = (40, 60)$ nm. Of course, for positions away from the central anti-node of the mode, the electric field strength is lower, reducing the coupling of the NC to the cavity. There will thus be a trade-off between Q and field strength.

For a 20 nm diamond NC, the Q factor is close to 10^5 , or about 90% of the maximum unperturbed Q of the cavity, regardless of NC position. We note that Jelezko et al. [16] observed 1.5 to 2 μs spin coherence times in 20 nm sized nanocrystallites of diamond. Our results show that an NC of this size has little effect on our cavity mode Q factor whether it is embedded in the middle or positioned on top, and therefore is a very promising candidate for cavity QED experiments, which we now discuss.

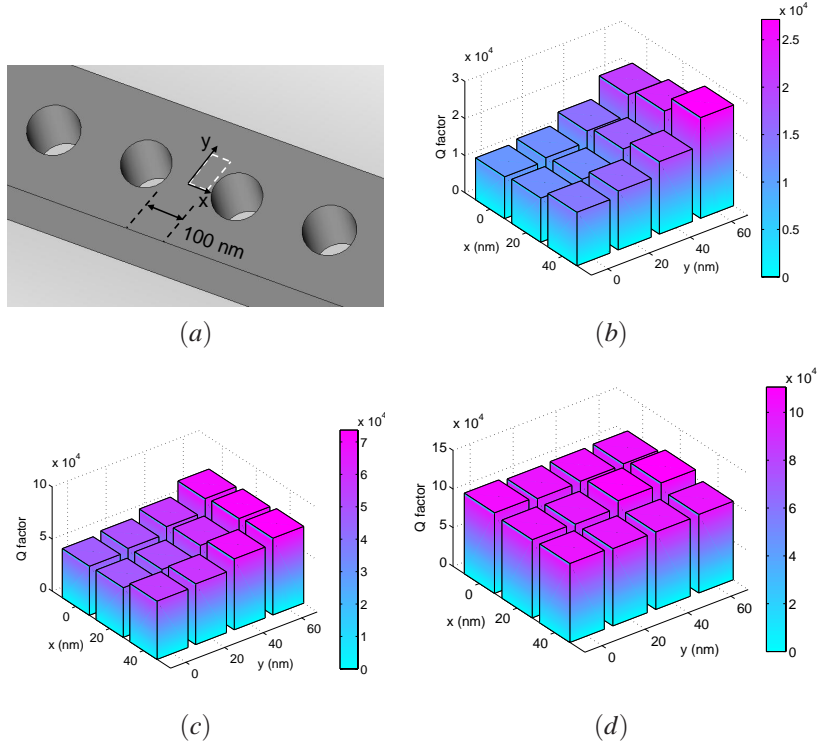


Fig. 3. Effect on the mode Q factor of a single diamond nanocrystal cube ($n = 2.43$) of varying size and displacement placed on top of the $s = 100$ nm 4-hole taper nanocavity, which has a maximum unperturbed Q of 115,000 (see Fig. 2(b)). The white box in (a) shows the range over which the nanocrystal is positioned, and the bar images show the Q factor as a function of position for NCs of size (b) 60 nm (c) 40 nm and (d) 20 nm. $(x, y) = (0, 0)$ denotes the nanocavity center (top surface).

4. Cavity QED analysis

To achieve strong coupling between a diamond NV center and a cavity, the coherent interaction rate, or vacuum Rabi frequency g , must exceed the decoherence rates due to the cavity loss, κ , and the spontaneous emission rate, γ ; i.e., $g > \kappa, \gamma$. The Rabi frequency is defined as $g = \vec{\mu} \cdot \vec{E}_{1\text{ph}}/\hbar$, where $E_{1\text{ph}}$ is the single photon electric field strength. At the electric field maximum of the cavity mode,

$$E_{1\text{ph}} = \sqrt{\frac{\hbar\omega}{2\epsilon_0 n^2 V}}, \quad (1)$$

where ω is the mode frequency, V is the mode volume, and $n = n_c$ is the cavity refractive index.

The dipole moment of the NV center can be deduced from its spontaneous emission lifetime, $\tau \sim 20$ ns [47], by using Fermi's golden rule for an electric dipole transition [48, 49], which gives

$$\mu = \sqrt{\frac{3\pi\epsilon_0 c^3 \hbar}{\tau n_e \omega^3}}, \quad (2)$$

where $n_e = 2.43$ is the refractive index of the diamond nanocrystal. Note that this dipole moment is integrated over the entire spectrum of the NV emission, a point we shall return to below.

The Rabi frequency can be evaluated from equations 2 and 1 to give

$$g_0 = \sqrt{\frac{3\pi c^3}{2\tau\omega^2 n_e n_c^2 V}}. \quad (3)$$

The label g_0 indicates that this is the maximum coherent interaction rate, which holds if the NV center is positioned at the mode maximum and aligned with its dipole moment parallel to the field vector.

When the emitter is not located at the mode maximum - e.g. if it is positioned on top of the cavity, as sketched in Fig. 1 - g_0 must be scaled by $\eta = E_{\text{NV}}/E_m$, the relative strength of the electric field at the NV location (E_{NV}) compared to at the mode maximum (E_m). This factor can be obtained from our FDTD simulations, and for a 20 nm NC on top of the cavity, it is given by $\eta = 0.25$.

If the NV center is embedded at the center of the cavity where the mode peaks, there is still a reduced field strength inside the NC due to the larger dielectric constant of the diamond compared to the surrounding cavity material. Maxwell's equations dictate that the normal component of the electric field at the interface between two materials (labeled 1 and 2) satisfies the boundary condition $\epsilon_1 E_1 = \epsilon_2 E_2$. For the small perturbation posed by a sub-wavelength sized diamond nanocrystal, this picture will be more complicated than for a single interface between two bulk dielectrics (in which case the field would be scaled down by a factor $(2/2.43)^2 = 0.68$ in the higher index diamond NC). We can again determine η precisely from FDTD simulations, and for a 20 nm diamond NC at the middle of the cavity, η ranges from 0.85-0.90.

For each cavity (see e.g. Fig. 2(b)), we are now in a position to calculate the relevant cavity QED figures of merit, given by the three angular frequencies $g = \eta g_0$, $\kappa = \omega/2Q$, and $\gamma = 2\pi/20\text{ns}$. In a diamond NV center, the zero-phonon line only contributes about 5% of the total emission, the rest being emitted into the phonon sideband [10]. Therefore, only $\approx 5\%$ of the total emission is coupled to the cavity mode, and g must be scaled by $1/\sqrt{20}$.

These parameters are plotted in Fig. 4. The spontaneous emission rate γ is independent of cavity length. The Rabi frequency has a weak dependence on cavity length through ω_0 and V , both of which change slowly with length. The cavity field decay rate, κ , obviously depends strongly on cavity length, as it is proportional to $1/Q$. For the 4-hole taper cavities with lengths $s = 90 - 100$ nm (black), the condition $g > \kappa, \gamma$ is satisfied only for the NC embedded in the center of the cavity. For the 7-hole taper (red), however, the strong coupling criterion can be satisfied for both the embedded and top-positioned NCs. Furthermore, for the 7-hole cavity with the maximum Q factor, the single-atom cooperativity for an embedded NC is $C_c = g_c^2/\kappa\gamma = 325$, which is a promising figure-of-merit describing the strength of the matter-field interaction. For the NC on top of the cavity, $C_t = 6$.

In the weak coupling regime, in which the rate of cavity decoherence κ exceeds the coupling rate g , the spontaneous emission rate will be strongly enhanced by the Purcell effect. At a temperature of 1.8 K, the emission linewidth of the ZPL corresponds to a Q factor of a few 10^7 [50], which is much narrower than the cavity line, signifying that the full ZPL can be strongly enhanced given optimal coupling with the cavity mode. For the 7-hole cavity with $Q =$ with an embedded diamond NC, the Purcell factor $F_p = 3Q\eta^2(\lambda/n)^3/4\pi^2V = 10^5$, assuming the full spectral and polarization alignment of the NV transition dipole moment with the anti-node of the cavity mode. The relative field strength η at the NC position enters as a squared factor [48]. If the NC is positioned on top of the 7-hole taper cavity, the maximum attainable Purcell factor is about 7,000. The cavity is thus a highly promising device to enhance the photon production rate from an NV center.

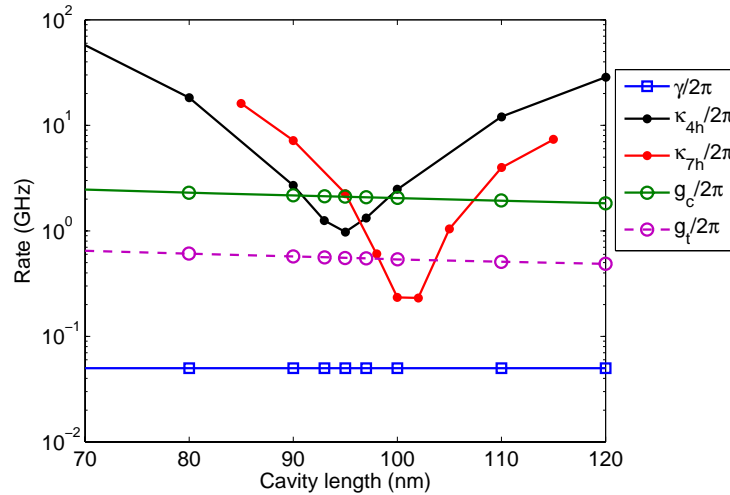


Fig. 4. Relevant cavity QED rates as a function of cavity length. $\gamma/2\pi$ is the spontaneous emission rate of the NV center, $\kappa/2\pi$ is the cavity decoherence rate with an embedded 20 nm NC (shown for the 4-hole and 7-hole taper cavities), and $g_c/2\pi$ ($g_t/2\pi$) is the Rabi frequency of the diamond NC embedded in the center (placed on top) of the cavity. For clarity, $g_c/2\pi$ and $g_t/2\pi$ are only plotted for the 4-hole taper cavity. They are not significantly different for the 7-hole taper cavity.

5. Conclusions

In this paper, we have designed a high- Q/V photonic crystal nanocavity with $n = 2.0$ for the purpose of strong coupling between the cavity mode and a single NV center in a 20 nm diamond nanocrystal. The structure should be relatively straightforward to fabricate, as the process is based on well-known nanofabrication techniques, and it naturally integrates the cavity with an on-chip ridge waveguide, allowing a well-defined output channel to be engineered for photons confined in the cavity mode [51]. This could be achieved either by shortening the photonic mirror to decrease the in-waveguide Q factor, or by applying a Q -spoiling pulse to inject free carriers into the cavity, as has been demonstrated in recent work on dynamic perturbations in photonic nanocavities [52, 53]. We have demonstrated a cavity Q factor of 1.4×10^6 with an effective mode volume of $0.78 (\lambda/n)^3$. We have shown that a 20 nm cubic diamond nanocrystal located either on the cavity surface or embedded within the cavity affects the Q factor by no more than 20% (in some cases for the better), and serves to reduce the mode volume by up to 20%. By calculating the Rabi frequency and comparing this to the decoherence rates of the system, we have shown that the optimal 7-hole taper cavity can operate in the strong coupling regime for both an embedded and a surface-positioned NC. We anticipate these results will open new avenues for photonic crystal-based visible photonics in both classical and quantum domains.

Acknowledgments

The authors thank Darrick E. Chang and Jennifer Choy for their insightful comments. Murray McCutcheon would like to thank the Natural Science and Engineering Research Council of Canada for its generous support. This work is supported in part by Harvard's National Science and Engineering Center (<http://www.nsec.harvard.edu>) and NSF NIRT grant ECCS-0708905.